Concept Design of Active Shielding for Dynamic Wireless Charging of Light-duty EV

Bo Zhang, Richard B. Carlson, Shawn D. Salisbury, Charles C. Dickerson, Timothy D. Pennington, Lee K. Walker and Eric J. Dufek
Department of Energy Storage and Advanced Transportation
Idaho National Laboratory
Idaho Falls, ID 83415
Email: bo.zhang@inl.gov; richard.carlson@inl.gov

***Abstract*— Dynamic wireless charging of electric vehicles is a flexible and state of the art charging technology with the potential capability of enabling fully automated in-motion charging. With charging power increasing to more than 100 kW for light duty vehicles, electromagnetic field (EMF) emission becomes a critical challenge. Due to the high costs of ferrite materials, this paper proposes an active shielding solution with multiple canceling coils installed on the ground side to supplement ferrite passive shielding to ensure electromagnetic safety. Two canceling coils are designed on two sides of the ground side coil. The canceling coils are small in size and 180 degree opposite in phase to the ground coil. Simulation and modeling shows that the canceling coils can reduce EMF emission from 37.2 µT to 18.2 µT at 0.8 m during 100 kW operation with only 2.5% of ground side current flowing in the canceling coils. These results have been preliminarily verified by inductance measurements and magnetic field measurement at 1.1 m distance without canceling coils. By further increasing the canceling coils' currents to 4%, EMF emission can also be mitigated at 200 kW, although the canceling coils' shape, position, and phase angle can be further optimized to improve the three-dimensional field distribution.**

Keywords—inductive power transfer, dynamic wireless power transfer, electric vehicle, electromagnetic field, active shielding

I. INTRODUCTION

Dynamic wireless power transfer (dWPT) or dynamic inductive power transfer (dIPT) is a newly developing, convenient, flexible, and state-of-the-art wireless charging technology [1-3]. Different from stationary inductive power transfer (IPT), in-motion wireless charging is the main technical feature for dIPT. For light-duty electric vehicle (LDEV) application, dIPT offers a good wireless charging solution for fully autonomous driving. More importantly, it offers the potential EVs to travel longer distances without requiring stops to recharge or increasing the size of the on-board battery, which brings potential benefit to reduce the requirement for battery energy storage capacity for LDEV [4, 5]. High power charging enables less of the roadway to be electrified in order to meet the vehicle energy requirements. The higher the power, the less ground side infrastructure is required resulting in lower capital costs and maintenance.

The state-of-the-art wireless charging technology for LDEV is currently approaching 100- to 200-kW level [6-8]. With the increase of wireless charging power, electromagnetic field (EMF) safety in regard to human health surrounding the dIPT becomes a critical concern [9]. [10] reports detailed impact evaluation of EMF on human body. Numerous existing investigations of suppressing stray EMF emission have mainly focused on coupler optimization or passive shielding design [11-13]. There have been some passive shielding solutions developed with ferrite that works well for stationary 100- to 200-kW level wireless charging [14]. However, due to the high cost of ferrite, it would be better to utilize less ferrite on the ground-side shielding solutions for IPT application scenarios.

In addition to passive ferrite shielding solution, active shielding by using canceling coils to mitigate leakage EMF is an alternative and cost-efficient method to achieve EMF safety. In several designs, shaped-ferrite was combined with canceling coils to actively mitigate leakage flux of dIPT [15, 16]. The canceling coils proposed were designed for heavy-duty vehicles (HDVs) in various large sizes/shapes which are not applicable for LDEV. One design, [17] installed two canceling coils next to both the primary and the secondary coils in order to supress stray magnetic field for stationary 1 kW IPT. [18] investigated the canceling coils' impact in reducing the coupling factor between primary and secondary coils. Since the adjacent canceling coils are large and impact the coupling factor, it's also not preferred for high power LDEV application.

This paper presents active shielding concept designs with multiple canceling coils installed to supplement ferrite passive shielding for a high-power (100- to 200-kW) dIPT system. An application scenario, a design consideration, and simulation results are presented in detail. Given the different technical features, this paper focuses on high-power dIPT for LDEVs; discussion of HDVs (e.g., trains, buses) [19, 20] is beyond the scope of this paper. Also, this paper focuses on the magnetic field. The electric field, which is typically not a critical concern for stationary IPT [21], is not discussed here and will be investigated for dIPT operation scenario in future studies.

II. Application Scenario and Concept Design

A. Multiple Active Canceling Coil Systems for dIPT

Fig. 1(a) presents a typical dIPT application scenario. In a specially planned electrified roadway lane, wireless charging pads are installed in the roadway. These series of charging pads are integrated with distributed power electronics supply, where high frequency resonant charging currents are provided. When LDEVs pass by, wireless pads are activated simultaneously and alternately to generate various EM fields which transfer the energy from the electric grid to the in-motion LDEVs and ultimately charge the LDEVs' batteries. During the charging process, the generated EM field for power transfer also creates stray EM field which might lead to safety concerns, hence the focus of this paper.

In addition to ferrite passive shielding presented in previous work [15], this paper presents an active shielding solution as a supplement to the main passive shielding to limit stray magnetic field, as shown in Fig. 1(b). Along the electrified lane, smaller canceling coils are installed on two sides of each ground-side coil. These canceling coils generate reverse magnetic fields simultaneously to the main fields from ground-side and vehicle-side coils to minimize stray magnetic field emissions at the edge of the electrified lane.

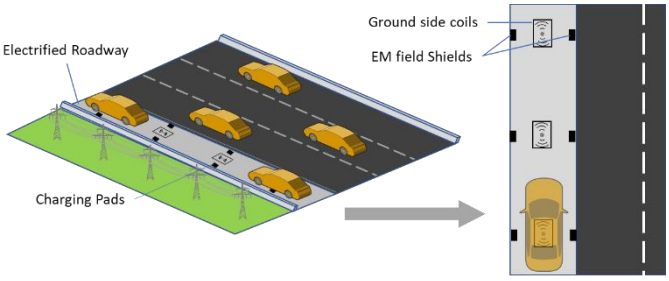

(a) (b)

Fig. 1. (a) Typical dIPT application scenario and (b) proposed active-shielding solution with canceling coils.

B. EM Safety Limitations

SAE J2954 defines a maximum allowed magnetic field of 27 μT at 0.8 m from the center of the vehicle-side coil for LDEV stationary IPT, as shown in Fig. 2 [23]. This standard is designed for stationary IPT where the 27-μT criteria comes from the ICNIRP 2010 standard [24] for human heath protection and the 0.8-m criteria is derived from a typical width of a 1.6-m wide LDEV.

No authority has yet defined a standard for EM safety distance (or magnitude) for dIPT. Definition of this standard is likely to be more complicated due to the realities of in-motion charging. Due to the higher risks posed by physical impact to a person or animal standing too close to a moving vehicle it is likely that the distance criteria should be larger than 0.8 m and may logically be at the edge of the driving lane (distance criteria to be half of the lane width). However, lane widths very drastically from the typical U.S. lane width of 3.7 m to the most narrow lane in Japan of only 2.75 m. Vehicles also vary in position within the lane and thus the distance from lane edge to center of vehicle-side coil will vary with different misalignments. Considering lane edge as an EM safety boundary for dIPT, the distance criteria between lane edge and center of vehicle-side coil is still an open question.

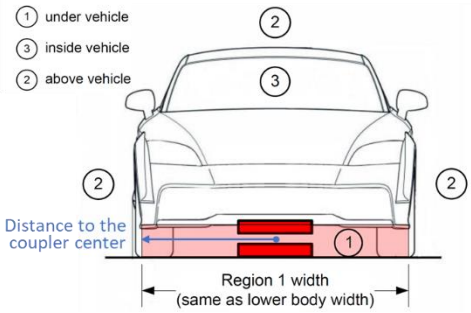

Fig. 2. Definition of magnetic-field emission limitations for LDEV in SAE J2954 [22].

III. Canceling Coil and Circuit Design

When an electric vehicle passes by a charging pad, the highest transferred power will be received when the vehicle-side coil and ground-side coil are aligned. To simplify, consider only the driver's safety aspect; the fully aligned situation is considered as the worst case because of the highest vehicle-side current received, although some misaligned scenarios might lead to higher EM emissions near the ground-side coils.

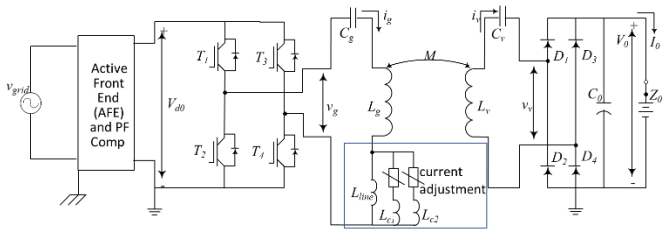

Fig. 3. The proposed dIPT circuit including two canceling coils in series with the ground-side coil.

Fig. 3 presents the proposed dIPT circuit, including two canceling coils in series with the ground-side coil. It consists of grid-voltage input, power-factor compensation, ground-side inverters, a ground-side compensation capacitor, a ground-side coil with attached ferrites, a vehicle-side compensation capacitor, a vehicle-side coil with attached ferrites, vehicle-side rectifiers, and a battery load, where v_g and v_v are the ground and vehicle-side transient voltages, respectively. Symbols i_g and i_v represent the ground- and vehicle-side transient currents, respectively; C_g and C_v stand for the ground- and vehicle-side compensation capacitors, respectively, and L_g and L_v present the ground- and vehicle-side coils, respectively. M is the mutual inductance between the ground- and vehicle-side coils, C_0 is the load-side bus capacitor, and Z_0 represents the equivalent DC-side load impedance. L_{c1} and L_{c2} are the two cancelling coils in series with the ground-side coil, where currents going through two cancelling coils L_{c1} and L_{c2} are adjustable and typically very low compared to the ground-side coil current. In this way, most of the currents (typically >95%) will still go through the ground-side coil and connected wire, which is presented as L_{line} in the circuit of Fig. 3, instead of through cancelling coils, so that the negative impact of losses on cancelling coils is minimized. To make the figure simple, different coils' inductance symbols L_g,

L_v, L_{c1}, L_{c2}, and L_{line} are used in Fig. 3 to present coils. Their resistances are also counted in the calculation, which will be presented in equations as follow.

The DC side load Z_0 in Fig. 3 can be transferred to AC-side equivalent impedance Z_{vac} as shown below [24, 25],

$$Z_{vac} = \frac{8}{\pi^2} Z_0 \tag{1}$$

Circuit equations based on a resonant circuit, shown in Fig. 3 can be given by:

$$v_g = \left(j\omega L_g + \frac{1}{j\omega C_g} + R_g + Z_c\right) i_g - j\omega M i_v \tag{2}$$

$$j\omega M i_g = \left(j\omega L_v + \frac{1}{j\omega C_v} + R_v + Z_{vac}\right) i_v \tag{3}$$

where R_g and R_v are corresponding resistances to L_g and L_v, respectively. Z_c presents the equivalent impedance of canceling coils' branch, which consists of two canceling coils' connected wires, as well as related current-adjustment equipment (e.g., switches, adjustable resistors, semiconductors), as marked in Fig. 3.

To make the canceling coils small overall, two canceling coils are connected, in parallel first, and then in series with the ground-side coil, as shown in Fig. 3, so that smaller Litz wire diameter, with lower current carriage capability, can be utilized compared to main coils. At this concept-design stage, the currents flowing in the canceling coils are simply set as 180 degrees opposite to the ground-side coil, which cancels most of the stray field generated next to the ground-side coils, although the phase differences between canceling coils and vehicle-side coils would be around 90 degrees.

In order to avoid affecting the coupling factor between ground-side and vehicle-side coils, two canceling coils are installed on two sides of the ground-side coil with large horizontal gaps so that the canceling coils and ground-side coil are decoupled, as shown in Fig. 4. In this way, the mutual inductance M can still be given by the following equation without canceling coils' impacts.

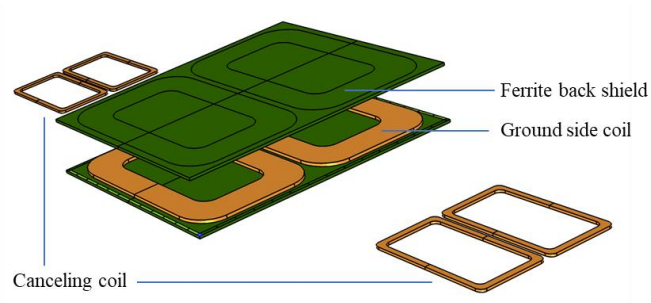

Fig. 4. The proposed two canceling coils' installation in series with the ground-side coil.

$$M = k\sqrt{L_p L_s} \tag{4}$$

where k is a coupling coefficient, typically between 0.1 and 0.5, owing to loose coupling [26]. Simulation calculations on mutual inductance between the ground-side coil and canceling coils will also be presented in the following section to ensure that canceling coils are decoupled from the two main coils.

Considering the resonant circuit, vehicle-side L-C and ground-side L-C are still resonant at the angular frequency ω_0, which meets the following equations:

$$j\omega_0(L_g + L_c) + \frac{1}{j\omega_0 C_g} = j\omega_0 L_v + \frac{1}{j\omega_0 C_v} = 0 \tag{5}$$

where L_c is the corresponding inductance component of Z_c.

Theoretically, the ground-side compensation capacitor C_g requires to be retuned to fully compensate the additional inductances coming from the two canceling coils in L_c based on Eq. (5). Because the required increase in C_g is typically too small to be able to find the next-level commercially available product, especially for high power IPT capacitor, this specific retuning process is practically omitted. To achieve this, L_c should be designed very small, to a negligible level compared to L_g so that the minor resonant-frequency differences between ground- and vehicle-side can also be ignored.

As a typical example of a high-power IPT, a 100-kW IPT system, with parameters described in [6], is adopted to carry out the simulations. Two canceling coils are located on the two sides of the ground-side coil at a distance of 0.8 m from the center of the ground-side coil. To minimize the impact of the canceling coils on the main circuits in terms of power losses in canceling coils and self-inductance increases for compensation capacitor-tuning consideration, only two turns are designed to wire the canceling coils with reverse low currents of 4.275 A, which is only 2.5% of the ground-side current. Table I summarizes the parameters of the designed canceling coils.

TABLE I
CANCELING COIL DESIGN FOR 100 KW IPT SYSTEM [6]

Quantity	Value
canceling coil turns	2
canceling coil current	4.275 A
canceling coil type	DD
resonant frequency	22 kHz
output power	100 kW
ground-side coil current	177 A
vehicle-side coil current	171 A
turns of ground or vehicle side coil	8
ground- or vehicle-side coil type	DD
ground- or vehicle-side coil shielding	backing ferrite

IV. SIMULATION RESULTS

Based on the circuit and canceling coils' design, presented previously, simulation verification is carried out in this section to prove the concept design. To ensure the simulation model's correctness, a finite-element model with parameters listed in Table I, without canceling coils, is preliminarily verified against measured self and mutual inductances, as well as magnetic-field measurement at 1.1 m distance, which will be presented in the following Subsections, A and B.

A. *Mutual-inductance decoupling check*

To ensure that canceling coils will not affect the main coils' coupling factor, mutual inductances between ground-side and vehicle-side coils, as well as those between ground-side and canceling coils are calculated by using finite-element simulation. In simulation, mutual inductance can be calculated based on Eq. (3) in case of a short circuit while self-inductance can be calculated, as below,

$$L_g = \frac{2E}{I_g^2} \tag{6}$$

where E is the total spatial EMF-energy integration when only one (e.g., the ground-side coil) is excited with all other coils in open circuit; I_g is the steady state RMS value of i_g. Table II presents the simulation results, along with part of measured self and mutual inductances. The canceling coils' hardware, as well as relevant current adjustment components, are still under development so their measured data are currently unavailable in Table II.

TABLE II
INDUCTANCES SIMULATION AND VERIFICATION

Quantity	Simulated Value (μH)	Measured Value (μH)
Self-inductance of ground-side coil	49.37	50.89
Mutual inductance between ground-side and vehicle sidle coils	22.46	22.43
Coupling factor between ground-side and vehicle sidle coils	0.46	0.44
Self-inductance of canceling coil	1.19	/
Mutual inductance between ground-side and canceling coils	1E-3	/
Coupling factor between ground-side and canceling coils	8.4E-4	/

The results compared in Lines 1–3 of Table II preliminarily illustrate the correctness of the simulation model because self and mutual inductances are major variables representing coils' EM energy-storage capability. The designed canceling coils only have 1.19 μH self inductance and 1E-3 μH mutual inductance with the ground-side coil; both are very small. These small inductance values support the previous discussion in Eq. (5) that canceling coils' inductances are designed to a negligible level compared to ground-side coil. In this way, the retuning procedure of compensation capacitors can practically be omitted due to the difficulties in capacitor-type selection with minor capacitance adjustments. The minor resonant-frequency differences between ground-side and vehicle-side can be ignored as well.

Comparing the mutual inductance of 22.46 μH between ground-side and vehicle-side coils to that of 1E-3 μH between ground-side and canceling coils, the canceling coil's impact on the coupling between the two main coils is negligible, which supports the discussion in Eq. (4) that the canceling coil will not affect IPT coupling effectiveness.

B. *Active shielding effectiveness*

Fig. 5 presents simulated results according to parameters listed in Table I with and without the canceling coils in blue and green lines, respectively, where the simulated magnetic field without canceling coils is preliminarily verified by a magnetic-field measurement at a 1.1-m distance with IPT operated at 100 kW. The distance to the center of the coils mentioned in all the following simulation results refers to the side-to-side direction along the mid-plane between ground- and vehicle-side coils of the vehicle, as shown in Fig. 2.

Canceling coils can reduce magnetic-field emissions from 37.2 to 18.2 μT at a 0.8-m distance from the center of the main coils. Also, all magnetic-field emission levels over 0.8 m are below the limit of 27 μT in accordance with ICNIRP 2010 [23]. Because only 2.5% of the ground-side current is flowing in the canceling coils, the downside of utilizing active canceling coils in terms of coil losses is acceptable. Note that 0.8 m marked here is just a reference as the worst case, which is not the distance criteria.

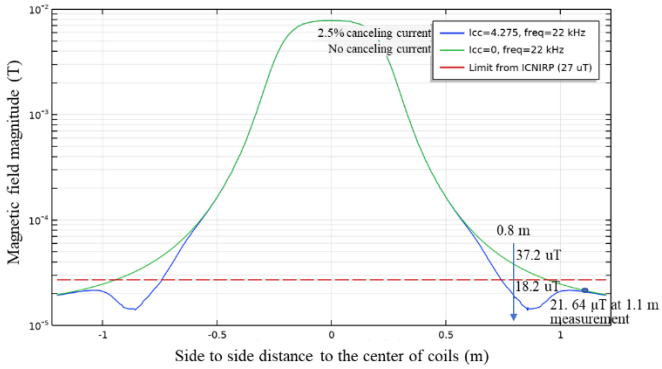

Fig. 5. Magnetic field shield effectiveness with and without canceling coils, operated in 100 kW.

In order to better understand canceling-coils performance in higher transferred power with different canceling-coil currents, simulations are also conducted at 200 kW operational power, with canceling-coil currents in 4, 2.5, and 0% of the ground-side coil current. Fig. 6 presents the simulation result. It is observed that the field emission around 0.8 m can still be limited to less than 27 μT in 200 kW operation by adjusting the flowing currents in the canceling coils. With canceling-coil currents increasing from 0 to 2.5 to 4%, the EM field at 0.8 m drops significantly from 53.2 to 25.8 to 13.1 μT, respectively.

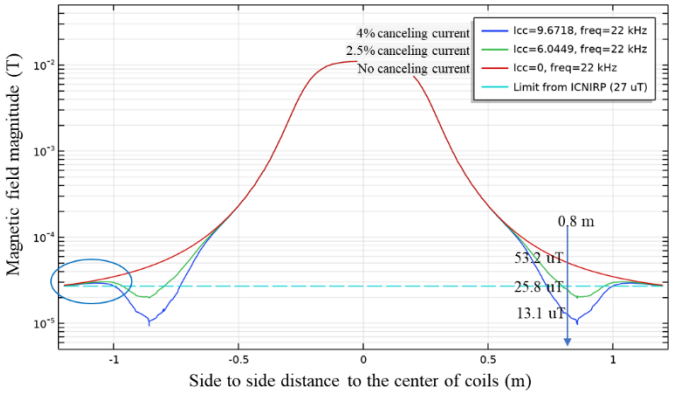

Fig. 6. Magnetic field shield effectiveness with different canceling coils' currents, operated in 200 kW.

On the other hand, Fig. 6 also demonstrates that canceling coils can only mitigate stray field within a limited region. The EM field emission outside of regions mitigated by canceling coils are still high, as marked by the blue circle of Fig. 6. This requires further investigation.

C. EM field distribution analysis

To clarify the canceling coils' impact on the surrounding EMF, field distribution in the mid-plane between ground- and vehicle-side coils is simulated. As a comparison, simulation result without canceling coils is provided. To be consistent with previous analysis results shown in Fig. 6, calculations are carried out in 200 kW operation, with all dimensional parameters in accordance with Table I. Also, only 2.5% of currents compared to that in the vehicle-side coil are flowing in canceling coils. The discussion here mainly focuses on the horizontal mid-plane while the vertical stray field, shown in Region 3 of Fig. 2, in accordance with SAE J2954 [22], is typically not of critical concern [21].

Fig. 7 presents a simulated magnetic-field distribution. Noting that the distribution is in mid-plane between the ground- and vehicle-side coils, in Fig. 7, the coils, ferrites, and canceling-coil shapes represent ground-side, vehicle-side, and canceling-coil projections to the mid-plane. In Fig. 7 (a), without canceling coils, the field distribution is ideally symmetric, which decreases isotropically at further distances.

However, when canceling coils are used, field distribution distorts a bit around the canceling coils. Based on the Biot-Savart law, the magnetic-field vector generated by ground-side, vehicle-side, and canceling coils in a three-dimensional space can be given by:

$$\vec{B}_{sum} = \frac{\mu_0 i_g}{4\pi}\oint_{coil\_g}\frac{d\vec{l}\times\vec{r}_g}{r_g^2} + \frac{\mu_0 i_v}{4\pi}\oint_{coil\_v}\frac{d\vec{l}\times\vec{r}_v}{r_v^2} + \frac{\mu_0 i_c}{4\pi}\oint_{coil\_c}\frac{d\vec{l}\times\vec{r}_c}{r_c^2} \quad (7)$$

where *coil_g*, *coil_v*, and *coil_c* present the ground-side, vehicle-side and canceling coils' volume regions for integration calculation; $\vec{r}_g$, $\vec{r}_v$, and $\vec{r}_c$ represent the distance vectors between the ground-side, vehicle-side, canceling coils and target point, respectively, where the magnetic field is calculated. Because the focus region of the stray-EM field is mainly in Region 2 of Fig. 2, as defined in SAE J2954 [22], so μ_0 is used here. Although nonlinear ferrite materials exist in the region, its permeability is still linear below the field saturation limit of 410 mT at 100°C [7, 27]. Thus, the whole region can still be treated as a linear system for purposes of magnetic-field calculation.

Comparing Fig. 7 (a) and (b), it is observed that canceling coils significantly mitigate the stray field in the middle of the canceling coils' cover regions, as shown in the lower white circle of Fig. 7(b), which is also consistent with the results shown in Fig. 6. However, the canceling coils also bring a downside in that the field at the edge is augmented, as shown in the upper white circle of Fig. 7(b). This can be explained according to Eq. (7). The generated magnetic fields from canceling coils in the middle are exactly opposite to those from the ground- and vehicle-side coils due to the 180 degree phase differences in currents, so the field in the middle is reduced. But with these canceling-coil orientation and current settings, the field generated by canceling coils at the edge would be around 90 degrees different from that generated from vehicle-side and ground-side coils, which ultimately enhances the stray field.

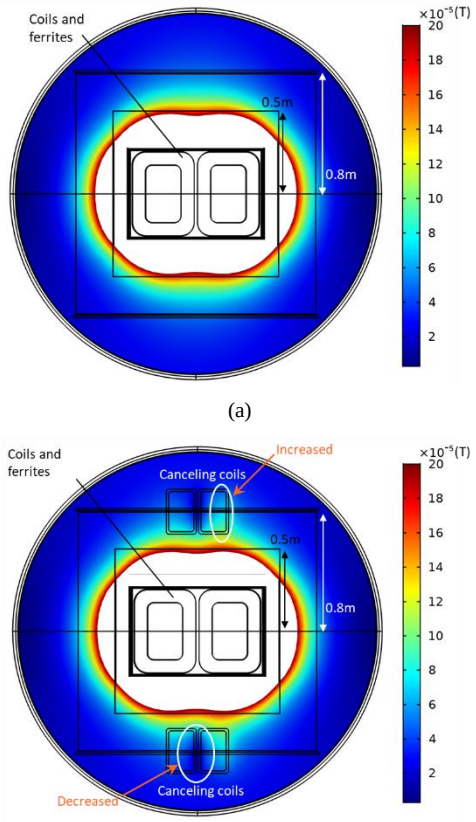

Fig. 7. EM-field distribution in mid-plane between the ground- and vehicle-side coils, operated at 200 kW. (a) Simulated results without canceling coils and (b) simulated results with canceling coils.

To better understand the shape of canceling coils' impact on EM-field distribution, one more case study, with the canceling coils' orientation adjusted, is also conducted. In this case, all parameters and operation powers are still consistent with that in Fig. 7, except for a 90 degree orientation adjustment in canceling coils, as shown in Fig. 8.

Comparing Fig. 8 to Fig. 7 (b), it is observed that the field-decreased areas in the middle of canceling coils' cover regions are broadened, as shown in the lower white circle of Fig. 8. Also, the downsides of the augmented EM field at the edge is suppressed a bit, as shown in the upper white circle of Fig. 8. The overall shielding effectiveness, in terms of EM-field distribution, is improved, but work can be continued to understand canceling-coils size and position-sensitive analysis, canceling-coil phase optimization, and the open discussion question about what exactly the EM-field distance criteria should be for dynamic IPT application scenario for LDEVs.

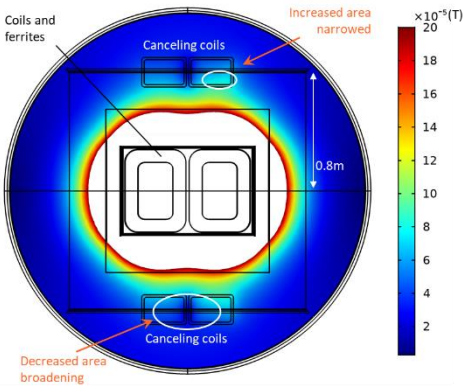

Fig. 8. Simulated EM field distribution in mid-plane between ground-side and vehicle-side coils when canceling coils rotate 90 degrees.

V. Conclusion and Discussion

dIPT is an emerging technology with the capability of enabling in-motion wireless charging. EMF safety is a critical concern as the charging power progresses beyond 100 kW. Due to the high cost and limited supply of high-performance ferrite materials, this paper presents an active shielding solution with multiple canceling coils as a supplement to passive ferrite to ensure EMF safety for 100–200 kW dIPT. A simulation model, which is preliminarily verified by inductance measurements and one-point magnetic-field measurements at 1.1 m for 100 kW, indicates that the proposed canceling-coil design can reduce EMF emission of 100 kW dIPT from 37.2 to 18.2 μT at 0.8 m from the center of main coils with only 2.5% of current flowing in the canceling coils. By further increasing canceling coils' currents to 4%, field emission can be mitigated below 27 μT when operated at 200 kW.

Active shielding research with canceling coils for dIPT is still at a concept-design stage. Because of the high cost and limited supply of high-performance ferrites, active shielding might serve as a good supplement in conjunction with passive ferrite shielding to reduce the amount of ferrite needed, even though some technical barriers remain and relevant disadvantages present in increasing system complexity. Further, canceling-coil shape, position optimization, co-simulation, and optimization with passive shielding, as well as phase-angle tuning studies are still under investigation. An on-site dIPT demonstration platform with LDEV is also planned to be built at American Center for Mobility (ACM) in Ypsilanti, MI [4]. This dIPT development and demonstration is lead by Oak Ridge National Laboratory, with partnership from Idaho National Laboratory, National Renewable Energy Laboratory, universities, and vehicle manufacturers. Due to the page limit of ITEC conference, more content will be presented in the future conference/journal publications. Additionally, the measurement distance for EMF safety criteria for dIPT application, considering different misalignments' scenarios, is still an open question given the range of roadway lane widths implemented around the world.

Acknowledgment

This work was supported by the U.S. Department of Energy (DOE), Vehicle Technologies Office, under the project FY2019 VTO AOI 3B: "High Power and Dynamic Wireless Charging for Electric Vehicles", with collaborative partners Oak Ridge National Laboratory (ORNL), Idaho National Laboratory, and National Renewable Energy Laboratory. All authors thank Veda Galigekere, Omer C. Onar, and Jason Pries from ORNL for their technical input, including IPT power electronics circuit design and EM field measurement data. The authors also thank Lee Slezak from U.S. DOE for project oversight and technical leadership.

References

[1] D. Patil, M. Mcdonough, J. Miller, B. Fahimi, and P. Balsara, "Wireless Power Transfer for Vehicular Applications: Overview and Challenges," IEEE Transactions on Transportation Electrification, Article vol. 4, no. 1, pp. 3-37, MAR 2018.

[2] G. Covic and J. Boys, "Inductive Power Transfer," Proceedings of the IEEE, Article vol. 101, no. 6, pp. 1276-1289, JUN 2013.

[3] Z. Zhang, H. Pang, A. Georgiadis, and C. Cecati, "Wireless Power Transfer-An Overview," IEEE Transactions on Industrial Electronics, Article vol. 66, no. 2, pp. 1044-1058, FEB 2019.

[4] C. Mi, G. Buja, S. Choi, and C. Rim, "Modern Advances in Wireless Power Transfer Systems for Roadway Powered Electric Vehicles," IEEE Transactions on Industrial Electronics, Article vol. 63, no. 10, pp. 6533-6545, OCT 2016.

[5] A. Azad, A. Echols, V. Kulyukin, R. Zane, and Z. Pantic, "Analysis, Optimization, and Demonstration of a Vehicular Detection System Intended for Dynamic Wireless Charging Applications," IEEE Transactions on Transportation Electrification, Article vol. 5, no. 1, pp. 147-161, MAR 2019.

[6] V. P. Galigekere et al., "Design and Implementation of an Optimized 100 kW Stationary Wireless Charging System for EV Battery Recharging," in 2018 IEEE Energy Conversion Congress and Exposition (ECCE), 23-27 Sept. 2018, pp. 3587-3592.

[7] J. Pries et al., "Coil Power Density Optimization and Trade-off Study for a 100kW Electric Vehicle IPT Wireless Charging System," in 2018 IEEE Energy Conversion Congress and Exposition (ECCE), 23-27 Sept. 2018, pp. 1196-1201.

[8] C. Zhang, S. Srdic, S. Lukic, Y. Kang, E. Choi, and E. Tafti, "A SiC-Based 100 kW High-Power-Density (34 kW/L) Electric Vehicle Traction Inverter," in 2018 IEEE Energy Conversion Congress and Exposition (ECCE), 23-27 Sept. 2018, pp. 3880-3885.

[9] B. Zhang, R. B. Carlson, J. G. Smart, E. J. Dufek, and B. Liaw, "Challenges of Future High Power Wireless Power Transfer for Light-duty Electric Vehicles----Technology and Risk Management," eTransportation, vol. 2, p. 100012, 2019.

[10] S. Park, "Evaluation of Electromagnetic Exposure During 85 kHz Wireless Power Transfer for Electric Vehicles," IEEE Transactions on Magnetics, Article vol. 54, no. 1, JAN 2018, Art no. ARTN 5100208.

[11] F. Lin, G. Covic, and J. Boys, "Leakage Flux Control of Mismatched IPT Systems," IEEE Transactions on Transportation Electrification, Article vol. 3, no. 2, pp. 474-487, JUN 2017.

[12] A. Ahmad, M. S. Alam, and A. A. S. Mohamed, "Design and Interoperability Analysis of Quadruple Pad Structure for Electric Vehicle Wireless Charging Application," IEEE Transactions on Transportation Electrification, pp. 1-1, 2019.

[13] L. Zhao, D. Thrimawithana, U. Madawala, A. Hu, and C. Mi, "A Misalignment-Tolerant Series-Hybrid Wireless EV Charging System With Integrated Magnetics," IEEE Transactions on Power Electronics, Article vol. 34, no. 2, pp. 1276-1285, FEB 2019.

[14] B. Zhang, R. B. Carlson, V. P. Galigekere, O. C. Onar, and J. L. Pries, " Electromagnetic Shielding Design for 200 kW Stationary Wireless Charging of Light-Duty EV," To be published in 2020 IEEE Energy Conversion Congress and Exposition(ECCE), 11-15 Oct. 2020, pp. 1-8.

[15] S. Choi, B. Gu, S. Lee, W. Lee, J. Huh, and C. Rim, "Generalized Active EMF Cancel Methods for Wireless Electric Vehicles," IEEE Transactions on Power Electronics, Article vol. 29, no. 11, pp. 5770-5783, NOV 2014.

[16] J. Shin et al., "Design and Implementation of Shaped Magnetic-Resonance-Based Wireless Power Transfer System for Roadway-Powered Moving Electric Vehicles," IEEE Transactions on Industrial Electronics, Article vol. 61, no. 3, pp. 1179-1192, MAR 2014.

[17] K. Furukawa, K. Kusaka, and J. Itoh, "General Analytical Model for Inductive Power Transfer System with EMF Canceling Coils," in 2018 International Power Electronics Conference (IPEC-Niigata 2018 -ECCE Asia), 20-24 May 2018, pp. 3349-3356.

[18] M. Mohammad, M. S. Haque, and S. Choi, "A Litz-Wire Based Passive Shield Design to limit EMF Emission from Wireless Charging System," in 2018 IEEE Energy Conversion Congress and Exposition (ECCE), 23-27 Sept. 2018, pp. 97-104.

[19] R. Bosshard and J. Kolar, "Multi-Objective Optimization of 50 kW/85 kHz IPT System for Public Transport," IEEE Journal of Emerging and Selected Topics in Power Electronics, Article vol. 4, no. 4, pp. 1370-1382, DEC 2016.

[20] K. Hwang, J. Cho, J. Park, D. Har, and S. Ahn, "Ferrite Position Identification System Operating With Wireless Power Transfer for Intelligent Train Position Detection," IEEE Transactions on Intelligent Transportation Systems, Article vol. 20, no. 1, pp. 374-382, JAN 2019.

[21] A. Mohamed, A. Meintz, P. Schrafel, and A. Calabro, "Testing and Assessment of EMFs and Touch Currents From 25-kW IPT System for Medium-Duty EVs," IEEE Transactions on Vehicular Technology, Article vol. 68, no. 8, pp. 7477-7487, AUG 2019.

[22] SAEJ2954, Wireless Power Transfer for Light-Duty Plug-In/Electric Vehicles and Alignment Methodology. [online] available: https://www.sae.org/standards/content/j2954_201904/, April 23, 2019.

[23] I. C. Non-Ionizing, "ICNIRP Statement-Guidelines for limiting exposure to time-varying electric and magnetic fields (1 Hz to 100 kHz)," Health Physics, Article vol. 99, no. 6, pp. 818-836, DEC 2010.

[24] V. Vorperian, "Simplified analysis of PWM converters using model of PWM switch. Continuous conduction mode," IEEE Transactions on Aerospace and Electronic Systems, Article vol. 26, no. 3, pp. 490-496, MAY 1990.

[25] H. Wu, A. Gilchrist, K. Sealy, and D. Bronson, "A High Efficiency 5 kW Inductive Charger for EVs Using Dual Side Control," IEEE Transactions on Industrial Informatics, Article vol. 8, no. 3, pp. 585-595, AUG 2012.

[26] V. Jiwariyavej, T. Imura, and Y. Hori, "Coupling Coefficients Estimation of Wireless Power Transfer System via Magnetic Resonance Coupling Using Information From Either Side of the System," IEEE Journal of Emerging and Selected Topics in Power Electronics, Article vol. 3, no. 1, pp. 191-200, MAR 2015.

[27] Ferroxcube. [online] available: https://www.ferroxcube.com/en-global/ak_material/index/power_conversion#5. (accessed March 1, 2020).

[28] ACM. American Center for Mobility, [online] available: https://www.acmwillowrun.org/. (accessed March 1, 2020).